Numerical Simulations of Outdoor Heat Stress Index and Heat Disorder Risk in the 23 Wards of Tokyo

Author(s): Yukitaka Ohashi, Yukihiro Kikegawa, Tomohiko Ihara and Nanami Sugiyama

Source: *Journal of Applied Meteorology and Climatology*, Vol. 53, No. 3 (March 2014), pp. 583-597

Published by: American Meteorological Society

Stable URL: https://www.jstor.org/stable/10.2307/26176326

Numerical Simulations of Outdoor Heat Stress Index and Heat Disorder Risk in the 23 Wards of Tokyo

YUKITAKA OHASHI

Faculty of Biosphere–Geosphere Science, Okayama University of Science, Okayama, Japan

YUKIHIRO KIKEGAWA

School of Science and Engineering, Meisei University, Hino, Tokyo, Japan

TOMOHIKO IHARA

Graduate School of Frontier Sciences, The University of Tokyo, Kashiwa, Chiba, and National Institute of Advanced Industrial Science and Technology, Tsukuba, Ibaraki, Japan

NANAMI SUGIYAMA

Faculty of Informatics, Okayama University of Science, Okayama, Japan

(Manuscript received 22 March 2013, in final form 26 November 2013)

ABSTRACT

In this study, the summertime outdoor heat stress hazard and heat disorder risks (HDR) were simulated numerically using a mesoscale meteorological model combined with an urban canopy model and a building energy model. Model grid maps including the 23 wards of Tokyo (23 Tokyo), Japan, were produced with a 1-km horizontal resolution for the period of July–September 2010. Model simulations of the daily maximum wet-bulb globe temperature ($WBGT_{max}$), which was adopted as a heat stress index, indicated the spatial heterogeneity of the heat stress hazard within 23 Tokyo. The heat stress hazard was greater in the inland western region, particularly for sunny conditions in July and August (based on the monthly mean; the maximum difference exceeded 2°C for both sunny and shaded conditions). This likely occurred as a result of greater spatial heterogeneity in the globe temperature than in the air temperature among model grid cells, with differences in the radiation environment induced by differences in urban geometric parameters. Gridded mapping of HDR simulations proceeded in two steps, using the incidence rate and the absolute number of heat disorder patients (HDP). These simulations were achieved by combining the exponential relationships between the actual $WBGT_{max}$ and the number of HDP with the daytime grid population. Eventually, the resulting HDR maps incorporated the effects of the spatial heterogeneities of both the outdoor heat stress hazard and the daytime grid population.

1. Introduction

In tropical and subtropical countries with extremely hot atmospheric conditions, human heat disorder (HD) is a severe problem. According to vital population statistics published by the Ministry of Health, Labor and Welfare (MHLW) in Japan, mortality related to HD in Japan has increased gradually from approximately 200 deaths in the second half of the 1990s to 1718 deaths in 2010 (MHLW 2010). Therefore, meteorological service companies and public organizations now provide numerical predictions of heat disorder risks (HDR) and daily heat advisories to residents.

In many countries, such bioclimatic predictions have been conducted for mesoscale spatial distribution (e.g., Matzarakis and Mayer 1997; Jendritzky et al. 2001; Błażejczyk and Matzarakis 2007; Fukuoka 2009; Kershaw and Millward 2012), utilizing many evaluation indices such as humidex, heat index, standard new effective temperature, physiological equivalent temperature, predicted mean vote, wet-bulb globe temperature

Corresponding author address: Yukitaka Ohashi, Faculty of Biosphere–Geosphere Science, Okayama University of Science, 1-1 Ridaicho, Okayama 700-0005, Japan.
E-mail: ohashi@big.ous.ac.jp

DOI: 10.1175/JAMC-D-13-0127.1

(WBGT), and universal thermal climate index. Moreover, mesoscale meteorological models are often utilized to predict and evaluate regional and continental human heat stress (e.g., Segal and Mahrer 1979; Segal and Pielke 1981; Tonouchi and Ono 2011). Such studies are advantageous in that they simulate spatial and temporal variations that consider meteorological conditions such as temperature, humidity, wind, and radiation. However, it is difficult to apply such meteorological variations over active surfaces within urban canopies. Although a computational fluid dynamics (CFD) model is expected to become available for the direct representation of urban district form (e.g., Murakami et al. 2000; Stathopoulos 2006; Ma et al. 2012; Moonen et al. 2012; Yoshida 2012), this model will be unsuitable for simulating human heat stress throughout a city over long periods of time because the associated calculation costs are not viable. Therefore, a simpler treatment and more realistic models are required to evaluate the spatiotemporal distribution of urban heat stress and hazards.

For hot environments that induce HD, the WBGT is often used as a heat stress indicator in various contexts, including military, industrial, domestic, sporting, and commercial applications (Parsons 2006). In fact, since being introduced as a guideline for heat stress and HD prevention by the American Conference for Governmental Industrial Hygienists (ACGIH) in the United States, the Health and Safety Executive (HSE) of the United Kingdom, and the Japan Sports Association (JASA), this index has been standardized as International Standards Organization (ISO) 7243 (ISO 1982; revised in 1989). However, some shortcomings of the WBGT have been highlighted, including its insufficient consideration of physiological parameters such as clothing, activity, and sweating in humans (e.g., Bernard et al. 2005; Budd 2008; Dehghan et al. 2012). Nevertheless, it has been reported that the WBGT correlates well with the number of heat-disorder patients (HDP) in Japan (e.g., Nakai et al. 1996; Hoshi and Inaba 2005; Asayama 2009). During summer in Japan, the number of HDP transported by ambulances increases rapidly when the daily maximum WBGT ($WBGT_{max}$) exceeds 26°–27°C (Hoshi et al. 2007; Ono 2009; Ohashi et al. 2011). Moreover, elevated numbers of HDP can persist in Japan for several months because extremely hot conditions often continue for long periods of time during the warm season (July–September), unlike heat-wave events that typically last for only several days. Therefore, maximizing the time for which human heat stress can be evaluated throughout an urban area is thought to be an effective strategy for the model prediction of heat hazard and HDR. Nevertheless, few studies have attempted simulation or prediction of regional HDR using numerical models (Gosling et al. 2009; Vanos et al. 2012); in particular, previous studies have neglected to develop applications to map the spatial distribution of heat hazard and HDR.

In the future, outdoor air temperatures and the actual heat stress will increase because of climate change and urban heat island intensification (e.g., Delworth et al. 1999; Diffenbaugh et al. 2007; Kusaka et al. 2012). Moreover, because the human body tends to become less efficient at thermoregulation with age, more elderly people have become susceptible to the influence of hot summer environments (e.g., Kenney and Munce 2003); the number of elderly people affected is expected to increase annually in Japan. Because these circumstances suggest the possibility of increased heat-related mortality in the future, predictions of future heat hazard and HDR due to climate change should be conducted hereafter (Lemke and KjellStrom 2012).

After consideration of the aforementioned background, the present study first developed numerical models for the quantitative evaluation of outdoor heat hazard and HDR using a gridded distribution within a broad urban area (the Tokyo metropolitan area in Japan) as the study area. Compared with CFD models, the use of which is limited to cases in which the simulation is implemented only over short time periods, the model presented here offers a particular advantage in that it can be used for successive evaluations of heat stress hazard and HDR throughout the hot months for an entire urban region. The newly developed model was used to simulate the WBGT and HDR grid maps with spatially heterogeneous distributions for Tokyo urban residents.

2. Heat disorder in Tokyo

In the present study, HDR grid maps were produced for the 23 wards of Tokyo (23 Tokyo), Japan. The population of 23 Tokyo was reported to have reached about 9 million by 2013, and the number of HDP transported by ambulances has been increasing annually in this region. Figure 1a illustrates the number of HDP and the number of HD deaths reported by Japanese public organizations [Ministry of the Environment (MOE), Government of Japan; Bureau of Social Welfare and Public Health, Tokyo Metropolitan Government] for 2006–11 in 23 Tokyo. Furthermore, Fig. 1b presents $WBGT_{max}$ averaged from July to September and for August only, as observed in Chiyoda Ward by the MOE. This figure demonstrates that the number of HDP and HD deaths vary widely on an annual basis. The most pronounced increases in these data occurred in 2010, with 3370 patients and 210 deaths. HD conditions were more extreme in 2010 than in other years as this year

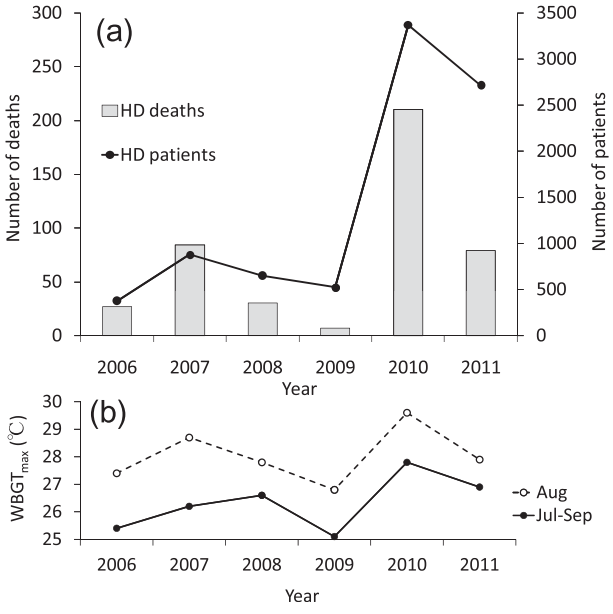

FIG. 1. Annual variations in the (a) number of HD deaths and HDP reported by MOE (Government of Japan) and the Bureau of Social Welfare and Public Health (Tokyo Metropolitan Government) during 2006–11 in 23 Tokyo and (b) $WBGT_{max}$ observed in Chiyoda Ward by MOE averaged over July–September and in August.

included many extremely hot days; in fact, annual $WBGT_{max}$ has been shown to correspond well in general with the yearly occurrence of HD. The rapid increase in HD deaths in 2010 is indicative of strong heat stress for residents in this year. Therefore, the simulations of the present study targeted outdoor heat stress and HDR in the hot season of 2010.

3. Model system

a. Models used in this study

A model system of the urban HDR was constructed by adopting several models: a mesoscale atmospheric model, an urban canopy model, and a building energy model. The model calculation flowchart is illustrated in Fig. 2.

The Weather Research and Forecasting (WRF) Model (Skamarock et al. 2008) is typically utilized to calculate mesoscale atmospheric conditions. The present study adopted version 3.0.0.1 of WRF, which is known as the Advanced Research WRF (ARW) and was developed by the National Center for Atmospheric Research. This numerical model is based on fluid dynamics equations with fully compressible fluid and non-hydrostatic equilibrium. The model physical parameterizations selected for radiation, cloud microphysics, planetary boundary layers, and land surfaces in the present study were the Dudhia shortwave (Dudhia 1989) and Rapid Radiative Transfer Model longwave (Mlawer et al. 1997) schemes, the WRF single-moment 6-class microphysics graupel scheme (WSM6; Hong and Lim 2006), the Mellor–Yamada–Janjić turbulent kinetic energy parameterization (Janjic 1994), and the Noah land-surface model (Chen and Dudhia 2001), respectively.

Urban meteorological conditions within an urban canopy layer can be calculated using the urban canopy model (CM), which was developed by Kondo and Liu (1998) and improved by Kondo et al. (2005). This model

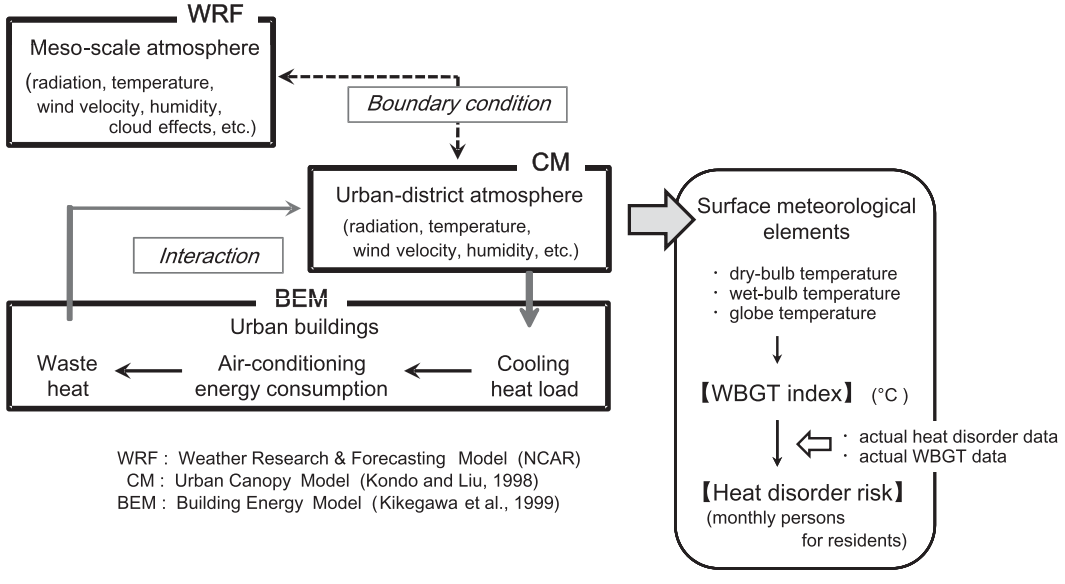

FIG. 2. Flowchart of the model calculation in the present study, which incorporates the WRF, CM, and BEM models.

assumes a vertically multilayered atmosphere that differs from the single-layer urban canopy of the WRF, and the primitive dynamics are vertically solved for a one-dimensional atmosphere. Therefore, it is assumed that uniform buildings represent subgrids of the WRF grids. However, building heights are typically evaluated by building density at each vertical level. Moreover, building and road widths averaged for any district area are generally given as urban morphological parameters. Wind speed, air temperature, and specific humidity are calculated only vertically. However, radiation conditions within the canopy are calculated considering the three-dimensional geometry of buildings, including roofs, road surfaces, and eastern, western, southern, and northern sidewalls. Therefore, sensible and latent heat fluxes can be calculated for these surfaces. Moreover, the radiation calculations can produce sunny and shaded places on road and building surfaces based on relationships between building heights, road width, and solar position (although they do not consider the presence of trees). Further details of the CM configuration are provided by Kondo et al. (2005) and Ohashi et al. (2007).

A building energy model (BEM) was incorporated to allow consideration of the heat emitted into the CM atmosphere by air conditioning. In hot and humid summers, such as those in Japan, residents and workers typically operate air conditioners constantly. The BEM adopted was originally proposed by Kikegawa et al. (1999) and improved by Kikegawa et al. (2003) and calculates heat exchanges between buildings and the CM atmosphere. For simplicity, the BEM treats the heat budget on a single-room basis. The input elements for a given room include the following: the solar radiation transmitted from windows; the conductive heat through walls; convective heat flow; and internal heat generated by lighting, machines, and humans. The output elements from a room correspond primarily to the waste heat emitted from exterior units of air conditioners. The amount of electrical power consumed by air conditioning is added to the amount of waste heat emitted from the room. Then, the amount of waste heat is determined by the coefficient of performance of the air conditioners, which is preselected for each air conditioning type given in the BEM, and divided into sensible and latent heat components. The BEM configuration was described in more detail by Kikegawa et al. (2003), Ohashi et al. (2007), and Ihara et al. (2008).

b. Outdoor WBGT

The outdoor WBGT (°C) can be calculated from the following equation (Yaglou and Minard 1957):

$$\mathrm{WBGT} = 0.7T_w + 0.2T_g + 0.1T_d, \tag{1}$$

where T_d, T_g, and T_w are the dry-bulb temperature (°C), globe temperature (°C), and natural wet-bulb temperature (°C), respectively. Although T_d can be obtained directly from the CM calculations, T_g must be estimated in the CM from the heat budget equation of a globe thermometer as follows:

$$\pi r^2 R_{\mathrm{dir}} + 2\pi r^2 R_{\mathrm{diff}} + 2\pi r^2 R_{\mathrm{ref}} + 2\pi r^2 L_d + 2\pi r^2 L_u = 4\pi r^2 H + 4\pi r^2 \varepsilon\sigma (T_g + 273.15)^4, \tag{2}$$

where R_{dir} and R_{diff} are the direct and diffuse solar radiation from the sky, respectively. The term R_{ref} is the solar radiation reflected from the ground and building surfaces, and L_d and L_u are the infrared radiation from the atmosphere and ground/building surfaces, respectively. These variables ($\mathrm{W\,m^{-2}}$) are calculated by the CM. Furthermore, r and ε are the radius (0.15 m) and emissivity (0.95) of the globe thermometer, respectively, and σ is the Stefan–Boltzmann constant ($5.67 \times 10^{-8}\,\mathrm{W\,m^{-2}\,K^{-4}}$).

Finally, T_g can be obtained from Eq. (2) when the remaining sensible heat flux on the surface of the globe thermometer, H ($\mathrm{W\,m^{-2}}$), is determined according to Eq. (3) (Toriyama et al. 2001):

$$H = \rho c_p C_H U (T_g - T_d), \tag{3}$$

$$C_H = 0.019; \quad U > 2.0\,\mathrm{m\,s^{-1}},$$

$$C_H = 0.0156U^{-0.82}; \quad U \le 2.0\,\mathrm{m\,s^{-1}},$$

where U is the surface wind speed ($\mathrm{m\,s^{-1}}$), ρ is the air density ($\mathrm{kg\,m^{-3}}$), and c_p is the specific heat at constant pressure ($\mathrm{J\,kg^{-1}\,K^{-1}}$). The heat budget of the globe thermometer at a height of 1 m is solved for shaded and sunny locations within the model subgrid. Formations of shadows on road and building surfaces can be calculated from the geometric relationship between buildings and solar radiation in the CM. Input radiations to the globe thermometer are greatly reduced on shaded surfaces relative to sunny surfaces; accordingly, the globe temperatures calculated from Eq. (2) vary between sunny and shaded locations.

The wet-bulb temperature in Eq. (1) is also calculated by the CM model. However, this parameter must be corrected to compensate for the unventilated wet-bulb temperature under solar exposure (i.e., the natural wet-bulb temperature). This conversion was conducted using a preliminarily developed empirical regression equation with actual observational data of ventilated and shelter-covered wet-bulb temperatures and natural wet-bulb temperatures. The WBGT obtained from the above

TABLE 1. Hazard ranking of outdoor heat stress levels, which are divided by the WBGT values published by JASA and JSB. This table was summarized by modifying that of Asayama (2009). WBGT values are inclusive of the lower limits but exclusive of the upper limits.

	Sport activities		Daily living	
WBGT (°C)	Hazard ranking (JASA)	Notes	Hazard ranking (JSB)	Notes
≥31.0	Danger	Prohibit	Danger	There is a risk at any physical activity level
28.0–31.0	Severe warning	Heavy exercise should be prohibited	Severe warning	
25.0–28.0	Warning	Rest should be provided frequently	Warning	Medium physical activity level might lead to HD
21.0–25.0	Caution	Water should be consumed often	Caution	There is a risk with a high level of physical activity
<21.0	Almost safe	Sufficient water consumption is suggested		

estimations represents the value at a height of 1 m, which is the lowest vertical level of the CM grids. Moreover, the sunny and shaded WBGTs can each be output using T_g under sunny and shaded conditions, respectively.

In Japan, a few preventative HD guidelines are published on the basis of WBGT values (Table 1). The hazard rankings of outdoor heat stress levels for sporting activities and daily living, which are utilized widely to prevent summer HD in Japan, are determined by JASA and the Japanese Society of Biometeorology (JSB).

4. Numerical simulations

a. Calculation conditions

In the WRF, horizontal resolutions were set to 3 and 1 km in the broad and narrow domains, respectively (Fig. 3); these domains were two-way nested. The CM horizontally resolved 23 Tokyo with a 1-km grid cell, which was also two-way nested at the upper boundary with the WRF narrow domain. The vertical grids of the urban canopy layer were set by the CM at 1, 3, 6, and 9 m, and so on, with increasingly wider intervals.

Table 2 summarizes the setting parameters required for the CM and BEM calculations. Buildings were classified as office/commercial buildings, apartment houses, and wooden houses on the basis of Tokyo GIS metropolitan polygon data, and the dominant building type was selected for each CM grid cell. Figure 3 illustrates these building types and other surrounding land-use types distributed within the model's narrow domain. Grid populations during daytime are also shown in the figure. The district structure created by buildings within the model grid cell was represented by area-averaged building parameters such as building width, street width, and vertical floor density distribution; these parameters were also produced using the aforementioned GIS data. Vegetation and water coverage rates for the urban ground were estimated from Landsat satellite data.

In the BEM, corresponding values and settings were obtained with reference to the Energy Conservation Center, Japan (2005) and include the time schedules of air conditioning and internal heating, the type of air conditioning, and the location of external units for each building type. The waste heat originated from air conditioning was emitted from building roof areas or at each floor height as sensible and latent heat. The air-cooled (using electricity) and water-cooled (using city gas) air conditioners were operated at particular rates depending on building type; these rates were determined from actual equipment data for completed buildings (ELPAC; Japan Building Mechanical and Electrical Engineers Association) according to Kikegawa et al. (2005). The ratio of sensible heat to latent heat was calculated from the constituent ratio of the air conditioning equipment.

Numerical integration was started at 0000 Japan standard time (JST) 1 July 2010 and terminated at 2300 JST 30 September 2010.

b. Estimations of HDR

To develop HDR grid maps in the simulations of the present study, it is important to first understand the relationship between the actual recorded number of HDP and the measured $WBGT_{max}$ value. Data of daily HDP transported by ambulances were provided by the Tokyo Fire Department, whose ambulance crews confirmed patients as suffering from heat disorders. This dataset contains the daily number of HDP for each ward of Tokyo. In addition, long-term WBGT measurements have been obtained in Chiyoda and Nerima wards by MOE in Japan, and these are provided to the public as hourly WBGT values each day. Because such data can be used to describe the actual relationship between meteorological conditions and acute diseases such as meteoropathy, it will be interesting to note whether daily WBGT variation affects the number of HDP.

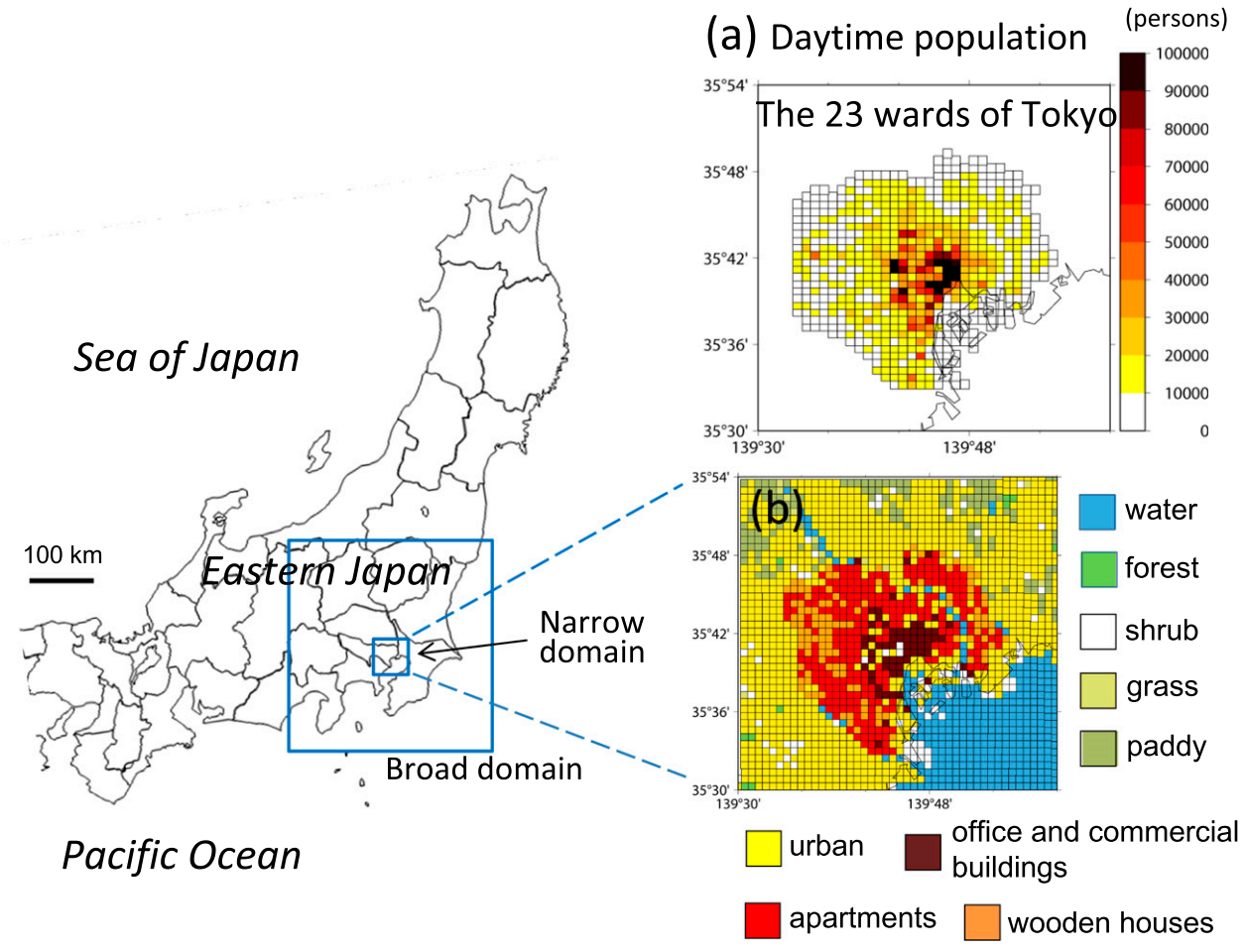

FIG. 3. Calculation domains (blue boxes) used in the simulations of this study. Simulation results in the narrow domain are analyzed. The (a) daytime population and (b) dominant land-use type within each 1-km grid cell in 23 Tokyo are also shown.

In the next step, the WBGT values simulated by the model were transformed into inferred HDR in cases where a clear relationship between the number of HDP and $WBGT_{max}$ was found in the measurement data. In the present study, the resident HDR within each grid cell was simulated. First, the HDR per daytime population of 100 000 (HDR_{ir}), which means the monthly incident rate of resident HD, was estimated by

TABLE 2. Input parameters required for the CM and BEM.

Building types	Office/commercial buildings, apartments, and wooden houses
District structure	Average building width, average street width, and building floor density (existence rate) in the vertical direction
Building surface types	Concrete, asphalt (only roads), window (only sidewalls), and vegetation (grass; on the street canyon)
Air conditioning	Setting temperature and relative humidity of room
	Operation duration
	Cooling type (air-cooled heat pump, water-cooled absorption hot and chilled water generator) and the coefficient of performance (COP)
	Ratio of possible air-conditioned floor area to total floor area
	Position of heat emission
Room conditions	Volumetric ventilation rate per unit floor area
	Floor area per unit worker and heat generated from a worker
	Sunlight transmissivity of windows
	Overall volumetric heat capacity of indoor air (including furniture and inner walls)

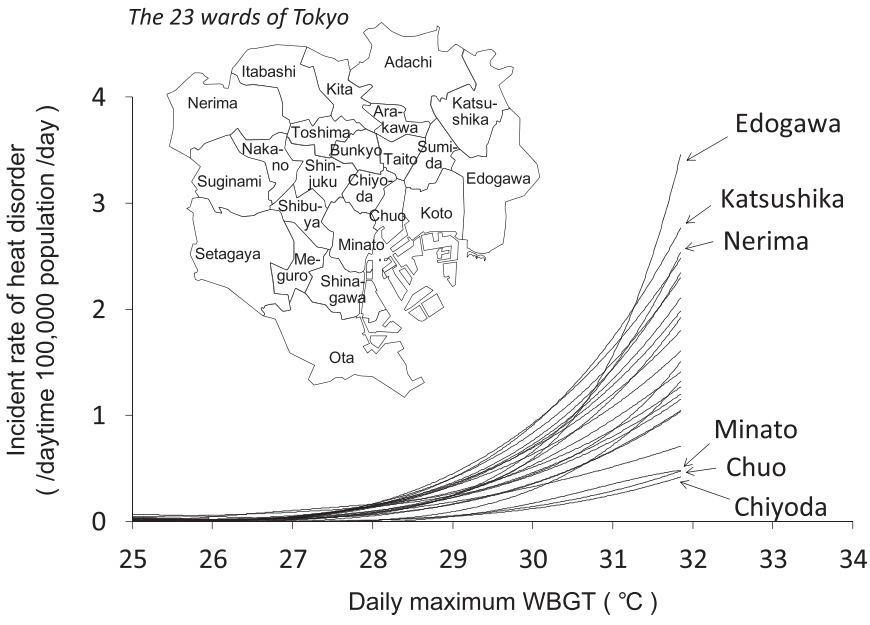

FIG. 4. Observed relationship between the incidence rate of HD (per daytime population of 100 000 per day) and $WBGT_{max}$ in each ward during the summer of 2010. The average $WBGT_{max}$ of the Chiyoda and Nerima wards was used here.

$$HDR_{ir} = \sum_{i=1}^{k} x_{ward\_i}. \quad (4)$$

Here, x_{ward_i} indicates the number of HDP transported by ambulances per daytime population of 100 000 in a given ward on the ith day, and k is the number of days in a given month. At this stage, population differences among grid cells were not reflected in HDR. Therefore, as the next step, HDR considering the daytime grid population (gp) (HDR_{abs}) for HDR_{ir} of Eq. (4) was calculated as follows:

$$HDR_{abs} = \sum_{i=1}^{k} \left(\frac{gp}{100\,000} x_{ward\_i} \right). \quad (5)$$

The variable x_{ward_i} in Eqs. (4) and (5) was derived at each model grid from the $WBGT_{max}$ values simulated by the numerical model, using a previously developed function for each ward (discussed in section 5a). Equations estimating x_{ward} were prepared for each of the 23 wards. These were polynomial equations describing the relationships between the actual number of HDP and the measured $WBGT_{max}$:

$$x_{ward} = aWBGT_{max}^6 + bWBGT_{max}^5 + cWBGT_{max}^4 + dWBGT_{max}^3 + eWBGT_{max}^2 + fWBGT_{max} + g, \quad (6)$$

where a, b, c, d, e, f, and g are constant values that were determined at each ward using actual data from 92 days during summer in 2010. Thereafter, these equations were assigned for each model grid according to the ward in which the grid cell was included.

In the grid map of the present study, 23 Tokyo was gridded at a resolution of 1 km. The gp values, determined using the 1-km resolution data for 2005 and 2006, were supplied by the Statistical Information Institute for Consulting and Analysis, Japan. As a result, after values of x_{ward_i} in each grid were obtained for sunny and shaded conditions using the calculated $WBGT_{max}$ in sunny and shaded conditions, respectively, both of these were added to obtain a total x_{ward_i} for each grid. Then, HDR grid values including sunny and shaded conditions were obtained using Eqs. (4) and (5). Finally, the HDR for each day were summed for each month (July, August, and September 2010). Therefore, the HDR_{ir} represents a risk with a unit of the monthly number of patients per daytime population of 100 000, whereas the HDR_{abs} represents that with a unit of the monthly absolute number of patients at each grid.

5. Results and discussion

a. Relationship between HDP and WBGT (observations)

Figure 4 illustrates the observed relationships between the incidence rate of HD (per daytime population of 100 000 in each ward per day) and $WBGT_{max}$ during the summer of 2010. These curves were determined by

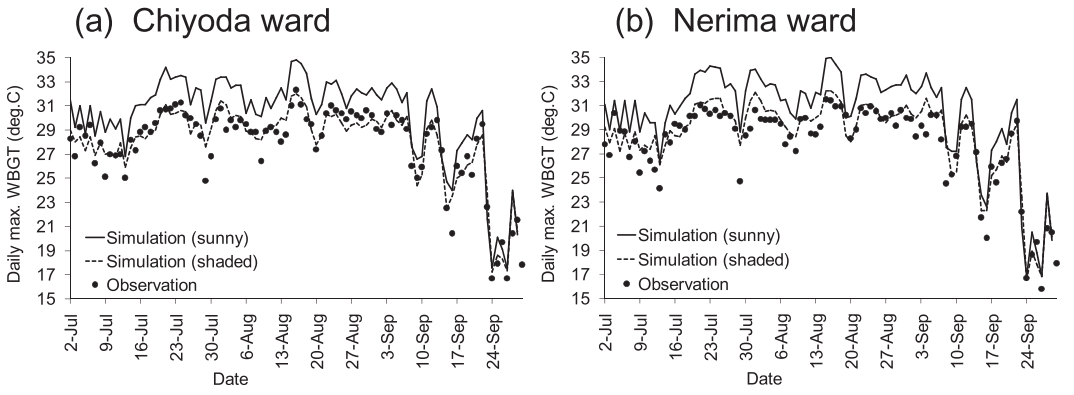

FIG. 5. Daily variations of $WBGT_{max}$ observed (dotted) and simulated sunny (solid) and shaded (dashed) conditions at grid cells within the (a) Chiyoda and (b) Nerima wards. These data were analyzed from 2 Jul to 29 Sep 2010.

Eq. (6) and utilized to estimate x_{ward_i} at each model grid, as described in section 4b. The average $WBGT_{max}$ of the aforementioned Chiyoda and Nerima wards was used for the analysis. The figure reveals that, although these curves differ by ward, the incidence rate of HD increased rapidly after the $WBGT_{max}$ value exceeded 27°–28°C; these values correspond to the "severe warning" ranking assigned by JASA and the JSB. Increases in the incidence rates of HD in the Minato, Chuo, and Chiyoda wards, with values of 0.4–0.5 at the $WBGT_{max}$ value of 32°C, were lower than those in the other wards. Conversely, these rates of the Edogawa, Katsushika, and Nerima wards increased more rapidly than in the other wards, where incidence rates were 2.4–3.5 at the $WBGT_{max}$ value of 32°C. The former wards are located at the center of the Tokyo metropolitan area, whereas the latter are located in surrounding or inland areas. Similar results were also observed for 2011: the Minato, Chuo, and Shinjuku wards at the center of the Tokyo metropolitan area exhibited slower increases in the incidence rates of HD, whereas the Katsushika, Nakano, and Setagaya wards in the surrounding or inland areas exhibited more rapid increases. Therefore, these results elucidate that the sensitivity of the rate of increase of the number of HDP to the outdoor $WBGT_{max}$ varies considerably among different wards.

b. *Comparison between simulation and observation results*

Validation of model simulation results is essential for discussion of the HDR simulation. Unfortunately, as previously stated, the routine WBGT measurements conducted by MOE were performed in only two regions of the Chiyoda and Nerima wards, which include coastal office buildings and inland wooden houses or apartments, respectively. Figure 5 presents comparisons of $WBGT_{max}$ values measured at these two wards with those calculated at the corresponding model grid. In the developed model, the WBGT was calculated for both sunny and shaded conditions for all grid cells. However, in the figure, there are a few days on which almost no difference in $WBGT_{max}$ between sunny and shaded calculations could be found. These days were included under cloudy conditions in the simulation. Simulated $WBGT_{max}$ reproduces well the actual variations measured at both wards. At Chiyoda (Nerima), the mean bias was +2.32°C (+2.45°C) and +0.18°C (+0.59°C) and the RMSE was 2.59°C (2.74°C) and 1.03°C (1.21°C) for sunny and shaded conditions, respectively. Based on analysis of each term of the WBGT equation [Eq. (1)], this positive bias likely occurred primarily because the calculated T_w was about 3°C higher than the observed value at the both sites for the August mean; however, the differences between calculated and observed values were less than 1° and 1.5°C for T_d and sunny T_g, respectively. This can be explained by the fact that the calculated T_w is calculated as the natural wet-bulb temperature, as stated previously, whereas the observed T_w is measured in a covered and ventilated shelter.

c. *WBGT grid maps*

Substituting $WBGT_{max}$ calculated by the model into the polynomial expressions for $WBGT_{max}$ and the HD population (section 4b) provided simulated HDR values for each model grid cell. Figure 6 shows grid maps of simulated monthly mean $WBGT_{max}$ from July to September 2010. Moreover, the $WBGT_{max}$ values were different under sunny and shaded conditions, owing to the abovementioned difference in the globe temperature calculation. Statistical results for the simulated $WBGT_{max}$ values are summarized in Table 3.

Figure 6 and the data in Table 3 indicate that the $WBGT_{max}$ levels varied significantly by month. The monthly $WBGT_{max}$ averaged throughout 23 Tokyo

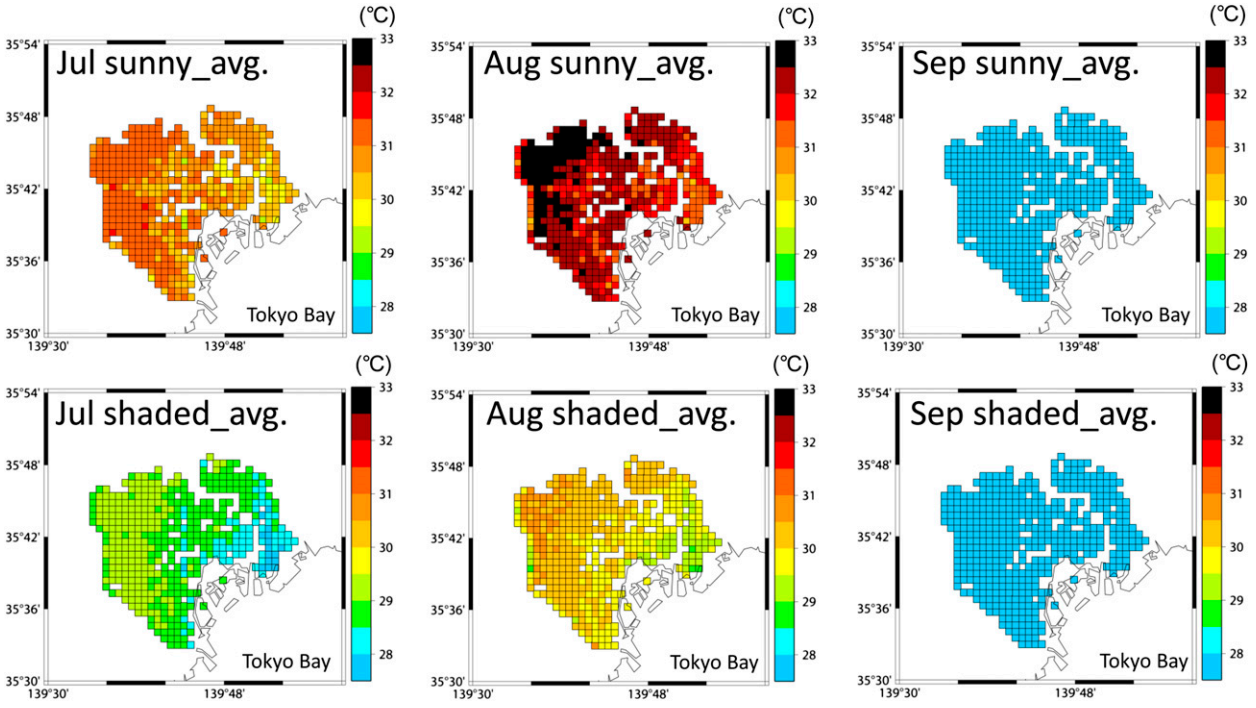

FIG. 6. Simulated grid maps of monthly mean $WBGT_{max}$ in July, August, and September 2010. The upper and lower panels correspond to results for sunny and shaded conditions, respectively.

was 30.8°C, 32.1°C, and 27.1°C in July, August, and September, respectively, in outdoor spaces under sunny conditions. The mean $WBGT_{max}$ for August was more than 31°C, meaning that August was assigned the strongest hazard ranking of ''danger''; this implies that outdoor workers, athletes, pedestrians, and all other residents were exposed to the threat of HD. The maximum and minimum values of the August mean $WBGT_{max}$ of the grids were 32.9° and 30.4°C, respectively; thus, model grid cells recording the ''danger'' ranking occupied approximately 98.3% of all grids. However, the ''danger'' grids in July occupied only 46.9% of all grids, which corresponds to about half of those in August. Under shaded conditions, the hazard ranking was reduced to ''severe warning'' ($WBGT_{max}$ = 28.0°–31.0°C), which is one category below the ''danger'' ranking, for almost the entirety of 23 Tokyo in July and August.

Conversely, all grid cells in September reflected a ''warning'' ranking with $WBGT_{max}$ values of 25.0°–28.0°C for both sunny and shaded conditions. A comparison of the September and August results revealed that the outdoor heat stress values varied significantly. The August $WBGT_{max}$ values indicated that almost all grids, even under shaded conditions, reached the ''severe warning'' ranking (28.0°–31.0°C); this indicates that people in the shade in August must pay more attention to HDR than people in sunny locations in September.

The simulated WBGT exhibited a wide spatial distribution (Fig. 6 and Table 3). For example, the highest mean $WBGT_{max}$ was recorded in August and was

TABLE 3. Summary of $WBGT_{max}$ simulations performed using the numerical model. Shown is the number of model grids, with the occupied percentage of all 458 grids in parentheses, by hazard ranking, along with the statistics.

		Hazard rankings of $WBGT_{max}$				Statistics of spatial $WBGT_{max}$ (°C)			
		Caution (21.0°–25.0°C)	Warning (25.0°–28.0°C)	Severe warning (28.0°–31.0°C)	Danger (≥31.0°C)	Avg	Max	Min	Std dev
Jul	Sunny conditions	0 (0.0%)	0 (0.0%)	243 (53.1%)	215 (46.9%)	30.8	31.6	29.1	0.48
	Shaded conditions	0 (0.0%)	16 (3.5%)	442 (96.5%)	0 (0.0%)	28.9	29.5	27.5	0.39
Aug	Sunny conditions	0 (0.0%)	0 (0.0%)	8 (1.7%)	450 (98.3%)	32.1	32.9	30.4	0.48
	Shaded conditions	0 (0.0%)	0 (0.0%)	458 (100.0%)	0 (0.0%)	30.0	30.8	28.7	0.39
Sep	Sunny conditions	0 (0.0%)	458 (100.0%)	0 (0.0%)	0 (0.0%)	27.1	27.7	26.3	0.23
	Shaded conditions	0 (0.0%)	458 (100.0%)	0 (0.0%)	0 (0.0%)	25.8	26.2	25.2	0.20

situated between the maximum $WBGT_{max}$ value of 32.9°C (northwest grid of 23 Tokyo) under sunny conditions and the minimum $WBGT_{max}$ of 28.7°C (southeast grid of 23 Tokyo) under shaded conditions; this difference exceeds 4°C. Moreover, even under the same sunny conditions, $WBGT_{max}$ exhibited maximum regional differences of 2.5°, 2.5°, and 1.4°C in July, August, and September, respectively, between the northwest and southeast regions in 23 Tokyo; under shaded conditions, the respective maximum differences were 2.0°, 2.1°, and 1.0°C.

Figure 7 shows the spatial distributions of T_d, T_w, and T_g, including each coefficient of the WBGT formula, for sunny conditions in August. It should be noted that the heterogeneity of T_g was greater than that of T_d and T_w, as evidenced by the highest standard deviation (0.33°C) and coefficient of variation (3.58%). In particular, considering the linear summation of the three terms, the spatial difference in the WBGT likely resulted from the wider range of the term of T_g (i.e., $0.2 \times T_g$) compared to the other terms; the terms T_d, T_w, and T_g showed variations of 0.13°, 0.21°, and 0.67°C, respectively, for a 1.0°C spatial difference in $WBGT_{max}$. Consequently, the outdoor WBGT distribution was affected particularly by the outdoor globe temperature, which primarily represented the radiation environment in the urban street canyon.

The reasons for the abovementioned heterogeneity and westward increase in T_g were clarified by a correlation analysis of T_g and other meteorological and urban geometric parameters. The results demonstrated that the spatial pattern of T_g in 23 Tokyo was correlated positively with the inward radiative flux ($R_{dir} + R_{diff} + R_{ref} + L_d + L_u$) to the globe thermometer and the sky-view factor ($r = 0.69$ with $p < 0.01$; $r = 0.29$ with $p < 0.01$, respectively). Such a correlation was not found for either T_d or T_w. In the western area of 23 Tokyo, where T_g was higher, low-rise wooden houses were the dominant type of structure (Fig. 3b); accordingly, larger sky-view factor grids were concentrated in this area. Thus, modeling the urban radiation environment appears to be significant in the evaluation of heat stress hazard using the WBGT. In other words, the existence of outdoor shading during the hot season can be reasonably effective at lowering heat stress and reducing HDR among residents and pedestrians. Lin et al. (2010) and Thorsson et al. (2011) presented calculations to demonstrate that the shading effect of buildings can reduce outdoor thermal discomfort in summer. The correlation analysis in the present study also demonstrates that the WBGT decreased with increasing average building height because of the shading effect on the road surface.

Muller et al. (2013) concluded that an increase in wind speed was the most effective adaptation measure in terms of improving thermal comfort, based on their CFD simulations for an actual urban district. Although the analysis presented here supports their results in that it indicates decreases in T_g and the WBGT with increasing average wind speed for the grid ($r = -0.63$ and -0.55, respectively), these quantities were not correlated with wind speed for weak-wind grids (August average of $<2\,m\,s^{-1}$) in the simulations of the present study. The area exhibiting this lack of correlation corresponds generally to the western area of 23 Tokyo that was specified previously.

d. HDR grid maps

Figure 8 illustrates numerical HDR maps estimated from $WBGT_{max}$ (i.e., Fig. 6) for each month. As was indicated in the WBGT maps of Fig. 6, the regional heterogeneity of HDR appeared in the results for July and August. Figures 8a–c present maps of HDR_{ir} and illustrate increases in this parameter of risk in the western part in 23 Tokyo, particularly in August. These spatial distributions were correlated strongly with those of $WBGT_{max}$, with a correlation coefficient of $r = 0.92$ in August. However, the spatial distribution of HDR_{abs} (Figs. 8d–f) appeared to approximate that of gp (shown in Fig. 3a) rather than that of $WBGT_{max}$, as evidenced by the respective correlation coefficients of $r = 0.97$ and 0.06 in August. This likely occurred because HDR_{abs} is proportional to the resident population inside the grid cell for reasons of population multiplication, as shown in Eq. (5).

Corresponding to the highest $WBGT_{max}$, the August HDR was higher than that for the other two months. The modal class of HDR_{ir} was 80–100, 120–140, and 60–80 HDP (the risk per daytime population of 100 000) in July, August, and September, respectively. The 120–140 HDP of the August simulation were found only rarely in July and September. For HDR_{abs} (i.e., the risk for the daytime grid population), a model grid value higher than 20 HDP existed for 215 grids and occupied 47% of the grid cells in August but only 14% and 8% of the grid cells in July and September, respectively. For the grid values, the maximum HDR reached 122.9, 299.2, and 88.3 HDP per month in July, August, and September, respectively.

The above discussion did not consider variations in HDR with age. However, body thermoregulation and daily activity vary among age classes such as children, working adults, and elderly people (e.g., Kenney and Munce 2003). Smoyer et al. (2000) demonstrated that mortality among the elderly was significantly higher on heat stress days than on other days in cities in southern Ontario in Canada. However, it was difficult to separate the age classes of HDP in the present study owing to

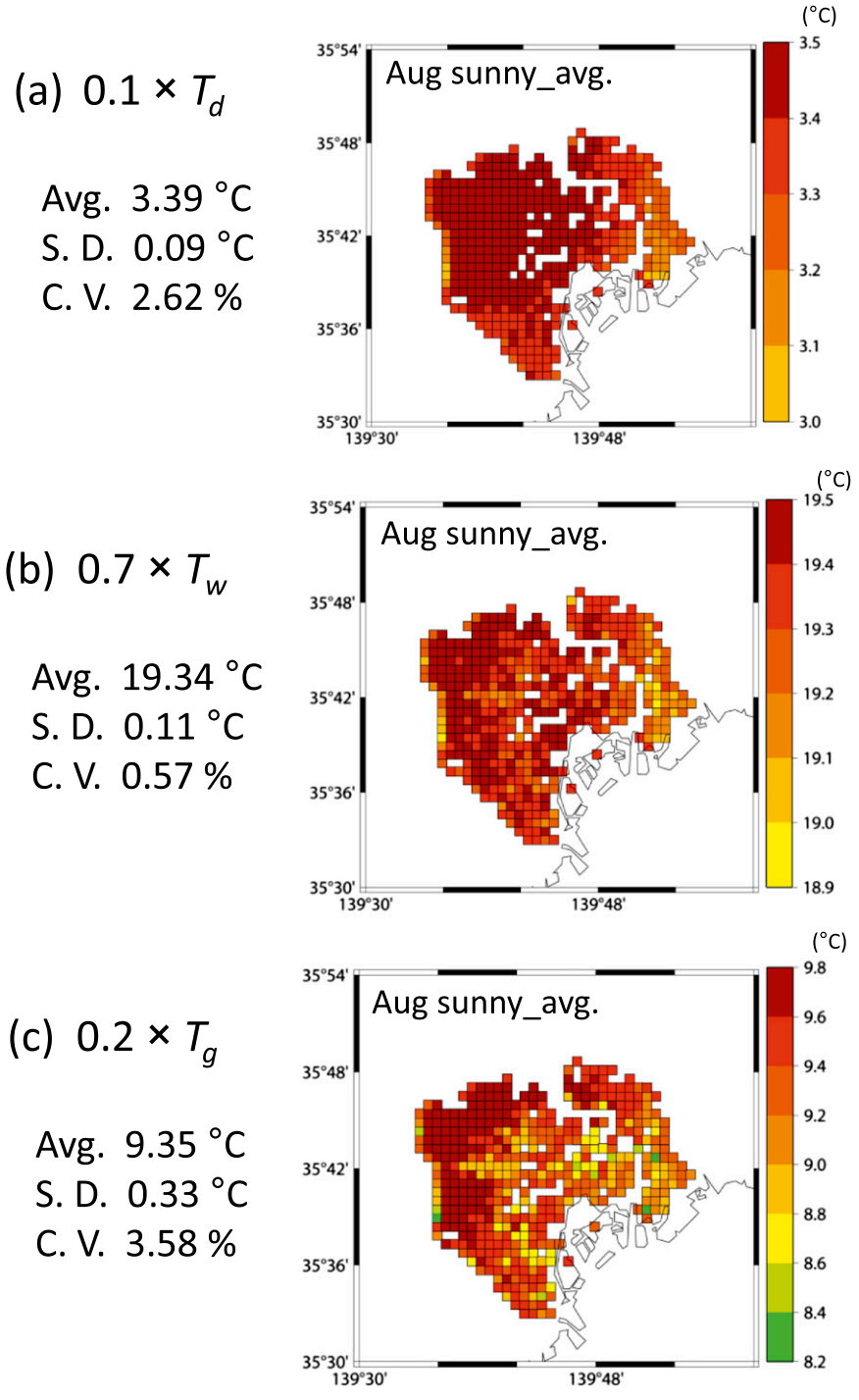

FIG. 7. Simulated grid maps for (a) 0.1 × T_d, (b) 0.7 × T_w, and (c) 0.2 × T_g (which make up the WBGT formula) for sunny conditions in August. Avg., S.D., and C.V. indicate spatial average, standard deviation, and coefficient of variation.

insufficient analysis data. Therefore, as HDR for heat-vulnerable children and elderly people are probably higher than those obtained here, additional analysis for age separation (e.g., consisting of HDR maps for each age class) will be required in future studies.

Figure 9 indicates the relationship between $WBGT_{max}$ (averaged for both sunny and shaded conditions) and HDR_{abs} in August divided at a gp boundary of 30 000. Grids with the gp of 30 000 or more were concentrated in the center of 23 Tokyo (see Fig. 3a). The results indicate

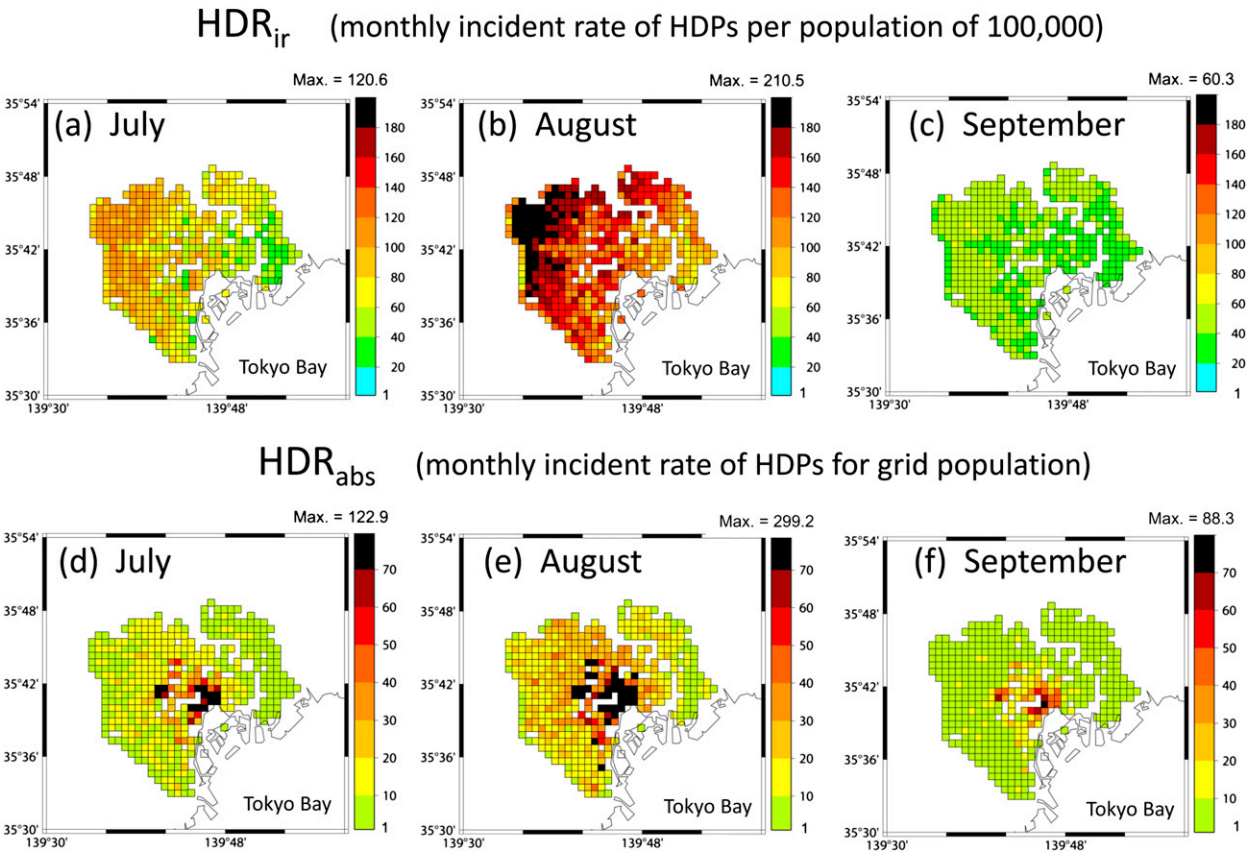

FIG. 8. Simulated grid maps of (a)–(c) HDR_{ir} and (d)–(f) HDR_{abs} for July, August, and September 2010.

that HDR_{abs} increased with $WBGT_{max}$ in the outer regions of 23 Tokyo, which consisted of grids with a gp of less than 30 000. Moreover, a comparison of Figs. 6 and 8e suggests that the higher $WBGT_{max}$ in the western region resulted in increased HDR_{abs} relative to that of the eastern region. Thus, the HDR_{abs} maps proposed in this study can successfully incorporate the influences of spatial distributions of both population and outdoor heat stress (i.e., the WBGT).

6. Summary

In the present study, the summertime outdoor heat stress and heat disorder risk (HDR) were simulated using a mesoscale meteorological model combined with an urban canopy model and a building energy model. Numerical grid maps covering the 23 wards of Tokyo (23 Tokyo) were produced with a 1-km horizontal resolution for the period spanning July–September 2010, which was an extremely hot season. Here, the outdoor heat stress hazard was represented by the wet-bulb globe temperature (WBGT). Then, the HDR at each grid cell was estimated by assigning the actual observed relationships between the daily maximum WBGT ($WBGT_{max}$) and the number of heat disorder patients (HDP) transported by ambulances. The results obtained in this study can be summarized as follows.

1) Analysis of actually observed $WBGT_{max}$ and HDP data revealed that the number of HDP increased exponentially with increasing $WBGT_{max}$. However, because the sensitivity of the number of HDP to $WBGT_{max}$ varied considerably among wards, the relationship between these parameters should be derived from local data as much as possible.
2) The spatial distributions of monthly mean $WBGT_{max}$ indicated the heterogeneity of heat hazard within 23 Tokyo. $WBGT_{max}$ tended to be higher in the western area, particularly in inland areas in the northwest. In both July and August, the spatial maximum difference of simulated monthly mean $WBGT_{max}$ was 2.5° and 2°C for sunny and shaded conditions, respectively. This difference reached 4°C in both months when both the sunny and shaded values were included.
3) Analyses of the sunny $WBGT_{max}$ in August indicated that model grid cells assigned to the ''danger'' ranking category ($WBGT_{max} \geq 31.0$°C), which was evaluated according to Japanese public guidelines,

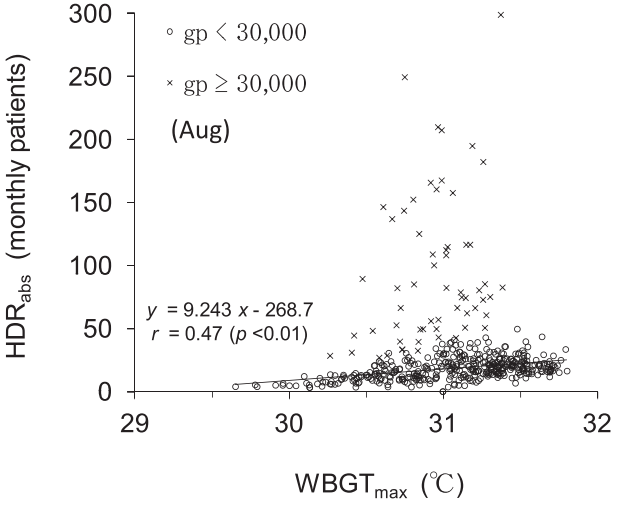

FIG. 9. Relationship between HDR_{abs} and $WBGT_{max}$ for August 2010. $WBGT_{max}$ is given as mean values for sunny and shaded conditions. The plots are divided at a gp boundary of 30 000 (circles, gp $<$ 30 000; crosses, gp $\geq$ 30 000).

occupied 98.3% of all grids; conversely, those in July occupied only 46.9% of the grids (i.e., about half the number of August). For shaded conditions, the hazard ranking was reduced below the danger category to ''severe warning'' ($WBGT_{max}$ = 28.0°–31.0°C) in almost all of 23 Tokyo in July and August. The September heat stress hazard was within the ''warning'' ranking ($WBGT_{max}$ = 25.0°–28.0°C), which did not occur in July and August, for all sunny and shaded conditions.

4) The spatial heterogeneity of $WBGT_{max}$ in 23 Tokyo resulted from larger differences in the globe temperature than air temperature among grid cells. The higher globe temperature in the western inland part of 23 Tokyo, which induced higher $WBGT_{max}$, was attributed to greater inward radiative flux to human height because of the larger sky-view factor of the model grid.
5) Gridded HDR maps estimated from $WBGT_{max}$ were simulated from the perspective of outdoor residents at each grid cell. Finally, HDR maps were produced using the daytime populations of each grid and the HD incidence rate per daytime population of 100 000, which was then converted using polynomial equations describing the relationship between $WBGT_{max}$ and the number of HDP, as discussed in point 1. This method successfully achieved HDR simulation, incorporating the influences of the distributions of both the outdoor heat stress hazard and the daytime grid population.

The results of this study suggest that HD hazard and HDR can be decreased effectively by improving the radiation environment at human height, as evidenced by the spatial distributions of WBGT described in point 4 above.

In Japan, several municipalities execute WBGT monitoring and HD prevention plans to protect human health locally (Martinez et al. 2011). The local gridded model simulation proposed in the present study is expected to contribute to future prediction of human heat risk and evaluation of effective HD prevention for urban planning under local and global climate change. For instance, this model offers potential as an effective tool for quantitative evaluation of HDR changes in response to the implementation of mitigation scenarios (e.g., building greening, highly reflective coatings, and anthropogenic heat reduction) for urban heat islands.

Acknowledgments. We thank the anonymous reviewers and editor for providing many valuable comments that helped us improve the manuscript. This study was supported by KAKENHI (23710047), Study of Grants-in-Aid for Young Scientists (B) of the Japan Society for the Promotion of Science (JSPS). In addition, this study was conducted as part of a research project (principal researcher: Associate Professor Satoru Iizuka at Nagoya University) under the Research Program on Climate Change Adaptation (RECCA) by the Ministry of Education, Culture, Sports, Science and Technology (MEXT), Japan.

The analysis used statistics related to patients with heat stroke transported by ambulances in metropolitan Tokyo provided by the Tokyo Fire Department of the Tokyo Metropolitan Government. We thank Mr. Ryuji Yoshida and Dr. Tetsuya Takemi of Kyoto University for allowing us to review their program and for their valuable comments on our WRF calculations. We also appreciate the help provided by Mr. Kazuki Yamaguchi of the Tokyo Electric Power Co. Inc. in our CM and BEM improvements. The generic mapping tools (GMT) graphics system (Wessel and Smith 1998) was used to produce some figures.

REFERENCES

Asayama, M., 2009: Guideline for the prevention of heat disorder in Japan. *Global Environ. Res.,* **13,** 19–25.

Bernard, T. E., C. L. Luecke, S. W. Schwartz, K. S. Kirkland, and C. D. Ashley, 2005: WBGT clothing adjustments for four clothing ensembles under three relative humidity levels. *J. Occup. Environ. Hyg.,* **2,** 251–256.

Błażejczyk, K., and A. Matzarakis, 2007: Assessment of bioclimatic differentiation of Poland based on the human heat balance. *Geogr. Pol.,* **80,** 63–82.

Budd, G. M., 2008: Wet-bulb globe temperature (WBGT)—Its history and its limitations. *J. Sci. Med. Sport,* **11,** 20–32.

Chen, F., and J. Dudhia, 2001: Coupling an advanced land surface–hydrology model with the Penn State–NCAR MM5 modeling system. Part I: Model implementation and sensitivity. *Mon. Wea. Rev.,* **129,** 569–585.

Dehghan, H., S. B. Mortazavi, M. J. Jafari, and M. R. Maracy, 2012: Combination of wet bulb globe temperature and heart rate in hot climatic conditions: The practical guidance for a better estimation of the heat strain. *Int. J. Environ. Health Eng.,* **1,** doi:10.4103/2277-9183.96006.

Delworth, T. L., J. D. Mahlman, and T. R. Knutson, 1999: Changes in heat index associated with CO_2-induced global warming. *Climatic Change,* **43,** 369–386.

Diffenbaugh, N. S., J. S. Pal, F. Giorgi, and X. Gao, 2007: Heat stress intensification in the Mediterranean climate change hotspot. *Geophys. Res. Lett.,* **34,** L11706, doi:10.1029/2007GL030000.

Dudhia, J., 1989: Numerical study of convection observed during the winter monsoon experiment using a mesoscale two-dimensional model. *J. Atmos. Sci.,* **46,** 3077–3107.

Energy Conservation Center, Japan, 2005: Research report of effects of the energy conservation on mitigating the heat island phenomenon (in Japanese).

Fukuoka, Y., 2009: Review on practical use of weather forecasting for health in Japan and Germany. *Global Environ. Res.,* **13,** 49–54.

Gosling, S. N., G. R. McGregor, and J. A. Lowe, 2009: Climate change and heat-related mortality in six cities. Part 2: Climate model evaluation and projected impacts from changes in the mean and variability of temperature with climate change. *Int. J. Biometeor.,* **53,** 31–51.

Hong, S. Y., and J. O. J. Lim, 2006: The WRF single-moment 6-class microphysics scheme (WSM6). *J. Korean Meteor. Sci.,* **42,** 129–151.

Hoshi, A., and Y. Inaba, 2005: Meteorological conditions and sports deaths at school in Japan, 1993–1998. *Int. J. Biometeor.,* **49,** 224–231.

——, ——, and K. Murayama, 2007: Characteristics of incidence of heat disorders in Tokyo and Chiba-shi (in Japanese). *Japanese J. Biometeor.,* **44,** 3–11.

Ihara, T., Y. Kikegawa, K. Asahi, Y. Genchi, and H. Kondo, 2008: Changes in year-round air temperature and annual energy consumption in office building areas by urban heat-island countermeasures and energy-saving measures. *Appl. Energy,* **85,** 12–25.

ISO, 1982: Hot environments—Estimation of the heat stress on working man, based on the WBGT-index (wet bulb globe temperature). International Standards Organization Standard 7243.

Janjic, Z. I., 1994: The step-mountain eta coordinate model: Further developments of the convection, viscous sublayer, and turbulence closure schemes. *Mon. Wea. Rev.,* **122,** 927–945.

Jendritzky, J., A. Maarouf, and H. Staiger, 2001: Looking for a universal thermal climate index (UTCI) for outdoor applications. *Proc. Second Windsor Conf. on Thermal Comfort Standards for the Twenty-First Century,* Windsor, United Kingdom, NCEUB.

Kenney, W. L., and T. A. Munce, 2003: Invited review: Aging and human temperature regulation. *J. Appl. Physiol.,* **95,** 2598–2603.

Kershaw, S. E., and A. A. Millward, 2012: A spatio-temporal index for heat vulnerability assessment. *Environ. Monit. Assess.,* **184,** 7329–7342.

Kikegawa, Y., H. Kondo, and H. Yoshikado, 1999: A study of the dynamical interaction between thermal environment and building energy consumption in the urban canopy. *Proc. 15th Int. Congress of Biometeorology and Int. Conf. on Urban Climatology,* Sydney, Australia, International Society of Biometeorology and International Association for Urban Climate.

——, Y. Genchi, H. Yoshikado, and H. Kondo, 2003: Development of a numerical simulation system toward comprehensive assessments of urban warming countermeasures including their impacts upon the urban buildings' energy-demands. *Appl. Energy,* **76,** 449–466.

——, ——, and H. Kondo, 2005: Impacts of the component patterns of air conditioning system and power supply system in buildings upon urban thermal environment in summer (in Japanese). *Environ. Syst. Res.,* **33,** 189–197.

Kondo, H., and F. H. Liu, 1998: A study on the urban thermal environment obtained through one-dimensional urban canopy model (in Japanese). *J. Japan Soc. Atmos. Environ.,* **33,** 179–192.

——, Y. Genchi, Y. Kikegawa, Y. Ohashi, H. Yoshikado, and H. Komiyama, 2005: Development of a multi-layer urban canopy model for the analysis of energy consumption in a big city. *Bound.-Layer Meteor.,* **116,** 395–421.

Kusaka, H., M. Hara, and Y. Takane, 2012: Urban climate projection by the WRF model at 3-km horizontal grid increment: Dynamical downscaling and predicting heat stress in the 2070's August for Tokyo, Osaka, and Nagoya metropolises. *J. Meteor. Soc. Japan,* **90B,** 47–63.

Lemke, B., and T. KjellStrom, 2012: Calculating workplace WBGT from meteorological data: A tool for climate change assessment. *Ind. Health,* **50,** 267–278.

Lin, T. P., A. Matzarakis, and R. L. Hwang, 2010: Shading effect on long-term outdoor thermal comfort. *Build. Environ.,* **45,** 213–221.

Ma, J., X. Li, and Y. Zhu, 2012: A simplified method to predict the outdoor thermal environment in residential district. *Build. Simul.,* **5,** 157–167.

Martinez, G. S., C. Imai, and K. Masumo, 2011: Local heat stroke prevention plans in Japan: Characteristics and elements for public health adaptation to climate change. *Int. J. Environ. Res. Public Health,* **8,** 4563–4581.

Matzarakis, A., and H. Mayer, 1997: Heat stress in Greece. *Int. J. Biometeor.,* **41,** 34–39.

MHLW, cited 2010: Vital statistics monthly (approximate) (including annual total for December 22, 2010) (in Japanese). [Available online at http://www.mhlw.go.jp/toukei/saikin/hw/jinkou/geppo/m2010/12.html.]

Mlawer, E. J., S. J. Taubman, P. D. Brown, M. J. Iacono, and S. A. Clough, 1997: Radiative transfer for inhomogeneous atmosphere: RRTM, a validated correlated-*k* model for the longwave. *J. Geophys. Res.,* **102** (D14), 16 663–16 682.

Moonen, P., T. Defraeye, V. Dorer, B. Blocken, and J. Carmeliet, 2012: Urban physics: Effect of the micro-climate on comfort, health and energy demand. *Front. Archit. Res.,* **1,** 197–228.

Muller, N., W. Kuttler, and A. B. Barlag, 2013: Counteracting urban climate change: Adaptation measures and their effect on thermal comfort. *Theor. Appl. Climatol.,* **115,** 243–257, doi:10.1007/s00704-013-0890-4.

Murakami, S., S. Kato, and J. Zeng, 2000: Combined simulation of airflow, radiation and moisture transport for heat release from a human body. *Build. Environ.,* **35,** 489–500.

Nakai, S., K. Shinzato, and T. Morimoto, 1996: Epidemiological analysis of heat disorders in Japan—An analysis of gleaned cases from newspaper reports between 1990 and 1994 (in Japanese). *Japanese J. Biometeor.,* **33,** 71–77.

Ohashi, Y., Y. Genchi, Y. Kikegawa, H. Kondo, H. Yoshikado, and Y. Hirano, 2007: Influence of air-conditioning waste heat on air temperature in Tokyo office areas during summer: Numerical experiments using an urban canopy model coupled with a building energy model. *J. Appl. Meteor. Climatol.,* **46,** 66–81.

——, Y. Kikegawa, K. Yamaguchi, and T. Ihara, 2011: Risk assessments of outdoor hot environment using urban meteorological numerical model system. *Proc. Second Symp. on Environment and Health,* Seattle, WA, Amer. Meteor. Soc., P343A. [Available online at https://ams.confex.com/ams/91Annual/webprogram/Manuscript/Paper183928/ex-abstract.pdf.]

Ono, M., 2009: Global warming and heat disorders (in Japanese). *Global Environ. Res,,* **14,** 263–270.

Parsons, K., 2006: Heat stress Standard ISO 7243 and its global application. *Ind. Health,* **44,** 368–379.

Segal, M., and Y. Mahrer, 1979: Heat load conditions in Israel—A numerical mesoscale model study. *Int. J. Biometeor.,* **23,** 279–284.

——, and R. A. Pielke, 1981: Numerical model simulation of human biometeorological heat load conditions—Summer day case study for the Chesapeake Bay area. *J. Appl. Meteor.,* **20,** 735–749.

Skamarock, W. C., and Coauthors, 2008: A description of the Advanced Research WRF version 3. NCAR Tech. Note NCAR/TN-475+STR, 113 pp. [Available online at http://www.mmm.ucar.edu/wrf/users/docs/arw_v3_bw.pdf.]

Smoyer, K. E., D. G. C. Rainham, and J. N. Hewko, 2000: Heat-stress-related mortality in five cities in southern Ontario: 1980–1996. *Int. J. Biometeor.,* **44,** 190–197.

Stathopoulos, T., 2006: Pedestrian level winds and outdoor human comfort. *J. Wind Eng. Ind. Aerodyn.,* **94,** 769–780.

Thorsson, S., F. Lindberg, J. Bjorklund, B. Holmer, and D. Rayner, 2011: Potential changes in outdoor thermal comfort conditions in Gothenburg, Sweden due to climate change: The influence of urban geometry. *Int. J. Climatol.,* **31,** 324–335.

Tonouchi, M., and M. Ono, 2011: Estimation of WBGT with JMA products and information web site for heat stroke in Japan. *Proc. Second Symp. on Environment and Health,* Seattle, WA, Amer. Meteor. Soc., P343A. [Available online at https://ams.confex.com/ams/91Annual/webprogram/Manuscript/Paper181591/AMS91_2_haelth_341.pdf.]

Toriyama, A., N. Monji, Y. Aono, and K. Hamotani, 2001: Effects of foliage and sky view factor on the urban thermal environment (in Japanese). *J. Agric. Meteor.,* **57,** 21–27.

Vanos, J. K., J. S. Warland, and T. J. Gillespie, 2012: Human energy budget modeling in urban parks in Toronto and applications to emergency heat stress preparedness. *J. Appl. Meteor. Climatol.,* **51,** 1639–1653.

Wessel, P., and W. H. F. Smith, 1998: New, improved version of the generic mapping tools released. *Eos, Trans. Amer. Geophys. Union,* **79,** 579, doi:10.1029/98EO00426.

Yaglou, C. P., and D. Minard, 1957: Control of heat casualties at military training centers. *AMA Arch. Ind. Health,* **16,** 302–316.

Yoshida, S., 2012: Evaluation of measures for pedestrians adapting to outdoor thermal environment. Preprints, *Eighth Int. Conf. on Urban Climate,* Dublin, Ireland, International Association for Urban Climate.